Scaling Law of Poly(ethylene oxide) Chain Permeation through a Nanoporous Wall

Rudra Prosad Choudhury,[†,‡,§] Petrik Galvosas,[||] and Monika Schönhoff*[,†]

Institute of Physical Chemistry, Westfälische Wilhelms-Universität Münster, Corrensstrasse 30/36, D-48149 Münster, Germany, International NRW Graduate School of Chemistry (GSC-MS), 48149 Münster, Germany, and Faculty of Physics and Earth Science, University of Leipzig, D- 04103, Leipzig, Germany

Received: May 27, 2008; Revised Manuscript Received: July 22, 2008

This paper presents a study of the permeation of poly(ethylene oxide) (PEO) chains through the nanoporous wall of hollow polymeric capsules prepared by self-assembly of polyelectrolytes. We employ the method of pulsed field gradient (PFG) NMR diffusion to distinguish chains in different sites, i.e., in the capsule interior and free chains in the dispersion, by their respective diffusion coefficient. From a variation of the observation time, the time scale of the molecular exchange between both sites and thus the permeation rate constant is extracted from a two-site exchange model. Permeation rate constants show two different regimes with a different dependence on chain length. This suggests a transition between two different mechanisms of permeation as the molecular weight is increased. In either regime, the permeation time can be described by a scaling law $\tau \sim N^b$, with $b = {}^4/_3$ for short chains and $b = {}^1/_3$ for long chains. We discuss these exponents, which clearly differ from the theoretical predictions for chain translocation.

Introduction

The question of the permeation of a single chain through a nanopore has attracted major attention due to its relevance in membrane biological processes. A number of recent theoretical approaches have dealt with this problem, yielding scaling laws of the molecular weight dependence of the translocation time τ, either in undisturbed equilibrium systems, or for driven translocation of a chain through a pore.[1−4] The translocation process in an equilibrium situation, i.e., without an external force, has first been described as a pure diffusive process, however, with this simple approach, different scaling exponents n of the translocation time

$$\tau = aN^n \tag{1}$$

where a is a constant, with a chain length of N resulting. Within a Rouse model of chain diffusion through the pore, Sung and Park obtained $n = 3$,[2] whereas linear diffusion of monomers leads to $n = 2$.[1] Since furthermore, the translocation time should be larger than the Rouse time for the diffusion of an unrestricted chain, an exponent of at least $2\nu + 1$, with ν being the Flory parameter, was postulated.[5] Several Monte Carlo simulations dealt with this problem yielding different exponents, see for example references.[6,7] Finally, Dubbeldam et al. described the translocation as an anomalous diffusion process and yielded a universal description of the exponent that agreed with their MC simulations.[3] In addition, Huopaniemi found a crossover of scaling laws from $n = 2\nu$ for short chains to $n = 1 + \nu$ for long chains;[8] similarly Panja et al. described anomalous dynamics up to the Rouse time, and diffusive translocation for long chains.[9]

Experimental studies of translocation times are so far limited to systems where the chain is subject to a driving force. Some studies have been made on DNA, for example by employing force-driven translocation[10] or electrophoretically driven transport.[11] Here, we provide the first experimental study of the free permeation of a chain through a nanopore in an equilibrium situation.

To build the nanopores, polyelectrolyte multilayers (PEM), which form a novel type of polymeric nanoporous membrane, are employed. Hollow capsules made of PEM provide a large application potential in encapsulation and drug delivery.[12,13] A key issue for applications is the development of tunable properties of the wall,[14−17] thus, there is a large interest in experimental methods to study the wall permeability. Corresponding studies performed so far can be distinguished into size determining methods on the one hand and time scale determining methods on the other hand. Concerning the former, cutoff sizes for permeation have been extracted from studies of the permeation of low molecular weight probe molecules of varying size through free-standing planar membranes of PEM,[18,19] which yielded permeation cut-offs at molecular sizes between 1 and 2 nm. Pore size distributions were extracted from nuclear magnetic resonance cryoporometry experiments, where the center of the size distribution was between 1.2 and 1.5 nm.[20]

On the other hand, time scales of permeation can be determined either by time-dependent fluorescence imaging, or in NMR exchange experiments. The majority of previous permeation studies have employed laser confocal scanning microscopy (LCSM) on fluorescent probe molecules in dispersions of large (>μm) capsules, where the time dependence of the spatial dye distribution is followed in a nonequilibrium experiment. Typically, fast permeation is observed for small molecules and slow or no permeation for macromolecules.[21−23] NMR methods do not suffer from the requirement of a fluorescence label or the size limit for optical detection. Any molecule carrying a NMR-active nucleus can be studied in an equilibrium situation, which makes this method particularly suitable to study molecular exchange in colloidal systems[24−27]

* Corresponding author. E-mail: schoenho@uni-muenster.de. Telephone: +49-2518323419. Fax +49-2518329138.

† Institute of Physical Chemistry, Westfälische Wilhelms-Universität Münster.

‡ International NRW Graduate School of Chemistry (GSC-MS).

§ Current address: Lehrstuhl für Makromolekulare Chemie, RWTH Aachen, Worringerweg 1, D-52074 Aachen. E-mail: rudra@mc.rwth-aachen.de.

|| Faculty of Physics and Earth Science, University of Leipzig. E-mail: galvosas@physik.uni-leipzig.de.

10.1021/jp804680q CCC: $40.75
Published on Web 10/01/2008

or even cellular systems.[28−30] Concerning polyelectrolyte multilayer capsules, we have previously employed PFG-NMR to study dextrane in hollow capsule dispersions[31,32] and even small organic molecules, such as phenol, which adsorb into the wall.[33]

Materials and Methods

Materials. Poly(allylamine hydrochloride), PAH (M_w 70 000 g/mol), and poly(diallyldimethylammonium chloride), PDADMAC (M_w 100 000−150 000 g/mol), were purchased from Aldrich and used without further purification. Poly(sodium-4-styrenesulfonate), PSS (M_w 70 000 g/mol) was purchased from Sigma. The PSS was purified by filtration (pore size 20 μm), followed by dialysis (membrane cutoff M_w 10 000−20 000 g/mol) against pure water to remove low molecular weight fractions. Polyethylene oxide (PEO) standards with a narrow molecular weight distribution (polydispersity 1.15) of different molecular mass (1000−40 000 g/mol) were purchased from Fluka. The water used was purified through a ultra pure three-stage water purification system (Millipore, resistivity >18 MΩ.cm). Monodisperse silica particles with a radius of 200 nm were purchased from Microparticles GmbH (Berlin). Deuterium oxide (99.9% isotopic purity) was purchased from Aldrich. HF was purchased as 40% solution, from Grüssing. NaCl (AR grade) was obtained from Merck.

Capsule Formation. Hollow PAH/PSS capsules were prepared in two steps. In the first step assembly of multilayers on the surface of silica particle was performed by the layer-by-layer technique. Each polyelectrolyte layer was prepared by adsorption from the respective polyelectrolyte solution followed by removal of excess polyelectrolyte. Adsorption and subsequent washing cycles were carried out with the method of centrifugation. Details of the procedure were described earlier.[34] In brief, 0.2 wt % of polyelectrolyte was dissolved in 0.5 M solution of sodium chloride (NaCl). The concentration of the SiO_2 particle dispersions was 2 wt %. The first layer was made of PDADMAC by adding 5 mL dispersion to 30 mL polyelectrolyte solution and allowing adsorption under stirring for 15 min. Then, excess polyelectrolyte was removed by three successive cycles of centrifugation, supernatant removal, and redispersion in water. The same procedure of layer formation was repeated to form alternating layers of PSS and PAH, until a total of 10 layers was deposited. Each adsorption step was confirmed monitoring the particle size as well as the ζ-potential by a Zetasizer 300HSA and a Zetasizer 4 (both Malvern Instruments), respectively. In the next step, the silica core was removed to obtain hollow capsules. Silica was dissolved using dilute (0.5 M) hydrofluoric acid. The remaining capsules were washed in centrifugation-decant-redispersion steps until the pH of the decanted solution was neutral. The quality of the capsules was controlled by transmission electron microscopy (TEM). The volume fraction of the capsules in the sample reported here was calculated from the initial silica particle concentration, assuming negligible losses of particles during coating, and capsules during the core dissolution process. Finally, the water in the sample was exchanged for D_2O by six to seven washing cycles, and the final (nominal) capsule concentration was adjusted to 2% (vol), with 0.5% (wt) of added poly(ethylene oxide).

NMR Measurements. A Bruker 400 MHz Avance NMR spectrometer was used for all NMR measurements. Diffusion and relaxation measurements were done using a liquid state probe head (Bruker "Diff 30") providing pulsed field gradients of up to 1200 G/cm. All measurements were done at room temperature (22.5 °C). The sample temperature was controlled by adjusting the temperature of the gradient coil cooling circuit with the help of a water circulation unit (Haake). The spin−lattice relaxation time (T_1) was measured by the inversion recovery sequence [$\pi-\tau-\pi/2$-FID]. The spin−spin relaxation time (T_2) was measured by the Carr−Purcell−Meiboom−Gill (CPMG) sequence [$\pi/2-(\tau-\pi-\tau)_n-$echo]. The PFG-NMR experiments were done in a pulsed gradient stimulated echo (PGSTE) sequence [$\pi/2-\tau_1-\pi/2-T-\pi/2-\tau_1-$echo] in combination with gradient pulses of duration δ and strength g, applied during each delay τ_1. As a consequence of the pulse program, T_2 relaxation was active only during the delay time τ_1. The spin lattice relaxation mechanism (T_1) is the only relaxation process active during the delay T. The spacing between the two gradient pulses is the observation time Δ, which was varied between 7 and 360 ms keeping τ_1 constant (τ_1 = 5 ms). DRCOSY experiments were done according to a sequence developed by Callaghan et al.,[35,36] consisting of a combination of PGSTE and CPMG [$\pi/2-\tau_1-\pi/2-T-\pi/2-\tau_1-(\tau_2-\pi-\tau_2)_n-echo$] in combination with gradient pulses of duration δ and strength g, applied during each delay τ_1.[36] In the DRCOSY experiments, the gradient pulse spacing Δ was kept constant (Δ = 20 ms). Independent variation of n and g yielded a two-dimensional data set. The value of the maximum gradient strength and the values of n and τ_2 of the CPMG part were adjusted to fully attenuate the signal to zero. Data from DRCOSY measurements were processed by a two-dimensional inverse Laplace transformation into the T_2 and D domains employing the programs Prospa (Magritek, New Zealand) and MATLAB (The MathWorks, Inc.). During the inverse Laplace transformation, the signal from the very first few gradient steps was discarded in order to suppress any signal from water.

Theory of Exchange in Diffusion Experiments. In a diffusion experiment the measured echo intensity for an isolated spin in a homogeneous environment can be described by[37−39]

$$I(k) = I_0 \exp\left(-\frac{\Delta}{T_R}\right) \exp(-Dk) \tag{2}$$

where Δ is the observation time, T_R is the effective relaxation time, D is the self-diffusion coefficient, and k can be written as

$$k = \gamma^2 g^2 \delta^2 \left(\Delta - \frac{\delta}{3}\right) \tag{3}$$

where γ is the gyromagnetic ratio of the nucleus, g is the gradient strength and δ is the gradient pulse duration. In a PFG stimulated echo pulse sequence the effective relaxation time T_R is given by[24]

$$\frac{1}{T_R} = \frac{1}{\Delta}\left(\frac{2\tau_1}{T_2} + \frac{T}{T_1}\right) \tag{4}$$

In a system, where a molecule can exist in two separate sites A and B, exchange between the sites is affecting the above equations. In either site the molecule is characterized by a diffusion coefficient $D_{A,B}$ and the relaxation times $T_{1A,B}$ and $T_{2A,B}$. Here, we describe as site A the free PEO chains in solution with the above parameters identical to those of PEO in D_2O, and a mean residence time in this site, τ_A. As site B we describe PEO chains associated with a capsule, such that D_B is the diffusion coefficient of the encapsulated site, i.e. that of the capsule. The mean residence time in that state is τ_B. The probability of finding the molecule in a given site i is f_i given by

$$f_{A,B} = \frac{\tau_{A,B}}{\tau_A + \tau_B} \tag{5}$$

and an exchange time τ_{ex} can be defined as

$$\frac{1}{\tau_{ex}} = \frac{1}{\tau_A} + \frac{1}{\tau_B} \tag{6}$$

A mathematical model describing the effect of two-site exchange on the echo decay in diffusion experiments has been described by Kärger.[40] In the limit of short gradient pulses ($\delta \ll \Delta$) and taking into account that relaxation times might differ in both sites, the echo decay of a stimulated echo becomes

$$I(k) = p_A \exp(-kD_A') + p_B \exp(-kD_B') \tag{7}$$

where k is given by eq 3. p_A and p_B are apparent population fractions and D_A' and D_B' apparent diffusion coefficients. $D_{A,B}'$ are given by

$$D_{A,B}' = \frac{1}{2}\left\{(D_A + D_B) + \frac{\Delta}{k}\left(\frac{1}{T_{RA}} + \frac{1}{T_{RB}} + \frac{1}{\tau_B} + \frac{1}{\tau_A}\right) \mp \sqrt{\left[(D_B - D_A) + \frac{\Delta}{k}\left(\frac{1}{T_{RB}} - \frac{1}{T_{RA}} + \frac{1}{\tau_B} - \frac{1}{\tau_A}\right)\right]^2 + \frac{4\Delta^2}{\tau_A \tau_B k^2}}\right\} \tag{8}$$

Here, T_{RA} and T_{RB} are the effective relaxation times of the nucleus in site A or B, respectively, as given by eq 4. The apparent populations are given by[40]

$$p_B = 1 - p_A = \frac{1}{(D_B' - D_A')}\left\{f_A\left(D_A + \frac{\Delta}{T_{RA}k}\right) + f_B\left(D_B + \frac{\Delta}{T_{RB}k}\right) - D_A'\right\} \tag{9}$$

Two extreme cases of eq 6 to eq 8 can be considered: In slow exchange, where $\tau_A, \tau_B \gg \Delta$, the equations decouple to

$$I(k) = (1 - P_B)\exp(-kD_A) + P_B \exp(-kD_B) \tag{10}$$

where P_B is the population fraction of the spin in site B, influenced by the relaxation, which can be written as

$$P_{A,B} = f_{A,B}\exp(-\Delta/T_{RA,B}) \tag{11}$$

Thus, in slow exchange the experiment probes the individual diffusion coefficients of molecules in both sites separately. In fast exchange, where $\tau_A, \tau_B \ll \Delta$, the decay becomes monoexponential with an averaged diffusion coefficient $D = f_A D_A + f_B D_B$.

Results and Discussion

Polymer Solutions. As a characterization of the free, not encapsulated state of PEO, polymer solutions of 0.5% (wt) PEO in D_2O are investigated. The relaxation times, i.e. spin−lattice relaxation time (T_1) and spin−spin relaxation time (T_2), are given in Table 1. They do not show any molecular weight dependence. The fact that T_2 is slightly shorter than T_1, i.e., $R_2 = 1/T_2$ larger than $R_1 = 1/T_1$, demonstrates the presence of slow segmental motions, since very slow motions contribute to the relaxation rate R_2 by a term proportional to $J(0)$, the spectral density at zero frequency. This term does not occur in the expression for R_1, and thus R_1 is dominated by fast local motions like bond rotations. Therefore, in the range of molecular weights investigated, not only the fast local motions, but also the slow segmental motions are independent of the chain length.

TABLE 1: Relaxation Times and Diffusion Coefficients of PEO in D_2O

M_w (g/mol)	T_1 (s)	T_2 (s)	D (10^{-11} m^2 s^{-1})	R_H (nm)
1000			18 ± 0.2	1.1 ± 0.2
2000			12 ± 0.2	1.6 ± 0.3
4000			8.2 ± 0.1	2.4 ± 0.1
8000	0.73 ± 0.03	0.55 ± 0.05	5.6 ± 0.1	3.5 ± 0.2
12 000			4.8 ± 0.1	4.2 ± 0.2
20 000			3.2 ± 0.2	6.2 ± 0.3
40 000			2.2 ± 0.1	8.9 ± 0.2

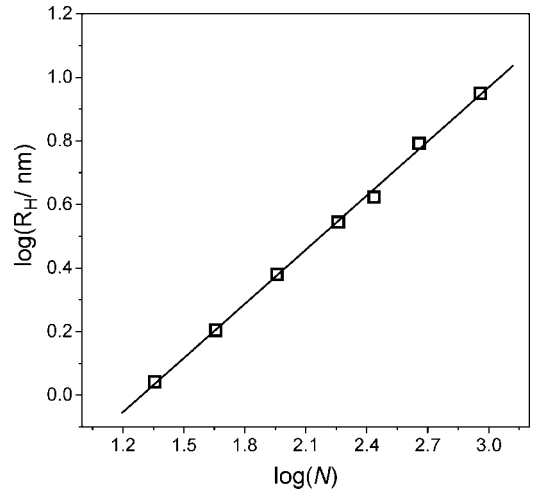

Figure 1. Hydrodynamic radii determined from diffusion coefficients by eq 12 (data points), and fit with eq 13 (solid line).

The diffusion coefficients show a strong dependence on the molecular weight of the polymer, see Table 1. All echo decay curves are monoexponential and experiments at different observation time, Δ, result in the same self-diffusion coefficient. Hydrodynamic radii are determined from the self-diffusion coefficients using the Stokes−Einstein equation

$$D = k_B T/6\pi\eta R_H \tag{12}$$

and are shown in Figure 1 in dependence on N, the number of monomer repeat units. A linear fit in the log−log representation assuming

$$R_H = aN^b \tag{13}$$

yields the scaling exponent $b = 0.57$. The agreement of the fit with the data points and the value of the exponent demonstrate that the chain conformation is well described by the model of a Gaussian chain with excluded volume.[41]

Diffusion of PEO in Capsule Dispersions. Figure 2 shows some selected echo decays of PEO in capsule dispersion for different molecular weights and different observation times. All samples exhibit biexponential echo decays, indicating the presence of two localizations of PEO with different diffusion coefficients. Corresponding independent biexponential fits of the echo decays for various observation time Δ yield apparent diffusion coefficients D_1 and D_2 for either site (see Table 2). Note, however, that the apparent diffusion coefficients D'_A and D'_B as defined by eqs 7 and 8 are distinctively different from D_1 and D_2 because of the additional constraint introduced by Δ.

The component with D_1 can be attributed to free chains in solution, see the agreement with the diffusion coefficients of free chains, Table 1. The other component diffuses slowly and D_2 does not strongly depend on molecular weight. This component can be attributed to a fraction of chains that is associated with or encapsulated in the capsules. We note that the size of the capsules is chosen small enough, such that any restricted diffusion of an encapsulated molecule can be neglected as compared to the diffusive displacement of the capsule itself in solution.

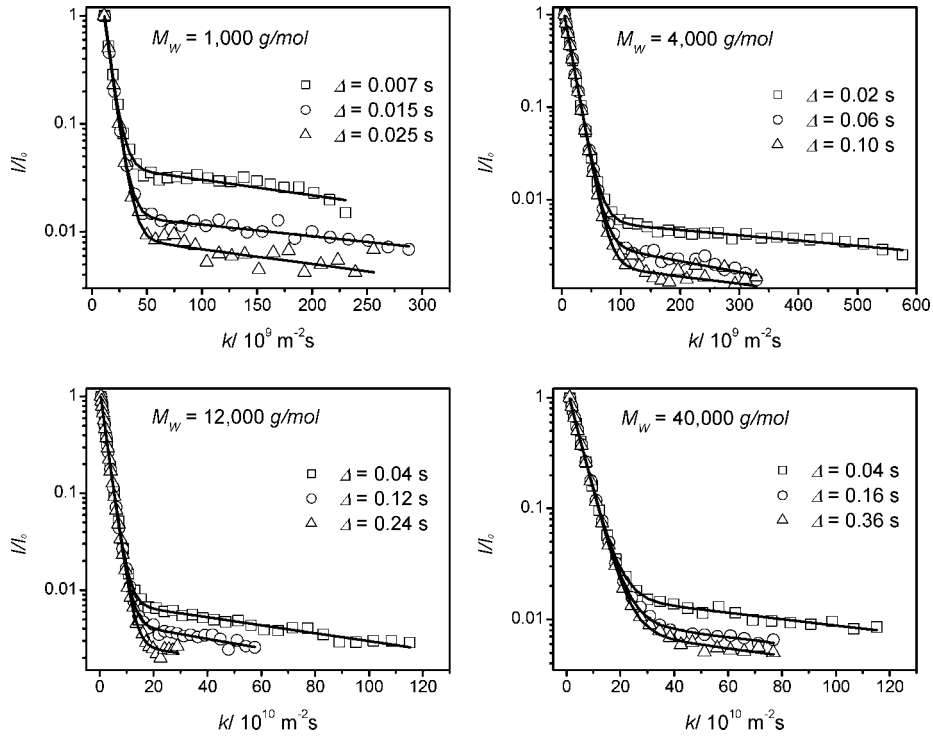

Figure 2. Echo decay curves of the PFG stimulated echo sequence at different molecular weight and different observation time. The solid lines are the result of biexponential fits to each decay curve.

TABLE 2: Relaxation Times and Apparent Diffusion Coefficients (Averaged with respect to Δ) of PEO in Capsule Dispersion

M_w (g/mol)	T_1 (s)	T_2 (s)	D_1 (10^{-11} m^2 s^{-1})	D_2 (10^{-13} m^2 s^{-1})
1000			17 ± 0.3	13 ± 0.6
2000			11 ± 0.3	13 ± 0.5
4000			8.1 ± 0.2	12 ± 0.5
8000	0.72 ± 0.03	0.45 ± 0.05	5.4 ± 0.2	12 ± 0.4
12 000			4.7 ± 0.2	9.6 ± 0.3
20 000			3.0 ± 0.1	9.6 ± 0.3
40 000			2.2 ± 0.1	9.8 ± 0.3

The biexponential behavior would point at a slow exchange between both sites with an exchange time $\tau_{ex} \ll \Delta$. However, as evident from Figure 2, with increasing observation time, the apparent fraction of the slow component is decreasing. This can either be attributed to a shorter relaxation time of the bound component, or to the influence of molecular exchange. The question of a possible shorter relaxation time of the bound component can be answered by relaxation measurements of PEO in capsule dispersion.

Both T_1 and T_2 relaxation experiments are showing one single component, the relaxation times are given in Table 2. T_1 of PEO in capsule dispersion is identical to that in D_2O. This indicates that the fast local motions are not affected by the presence of capsules. T_2 is similar to the value of free chains. However, since the fraction of encapsulated chains with a deviating T_2 might be small, it is possible that its influence on the experimentally determined overall value of T_2 is not evident within error.

To solve the question of the potential existence of a component with differing T_2, the correlation between diffusion coefficients and relaxation times was observed by diffusion relaxation correlation spectroscopy (DRCOSY).

DRCOSY. Diffusion-relaxation correlation spectroscopy was done on PEO in presence of capsule dispersion. Figure 3 gives an example of a DRCOSY spectrum of PEG (M_w = 8000 g/mol)

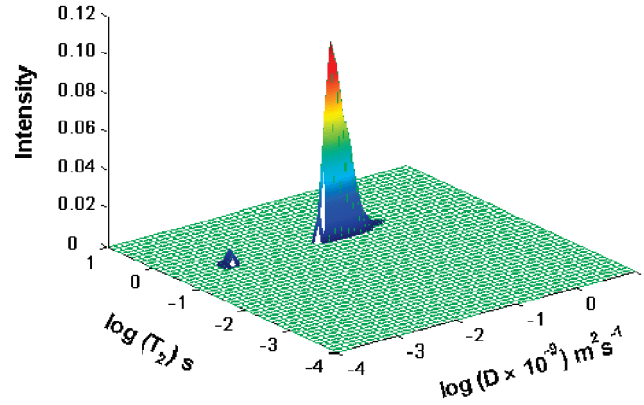

Figure 3. DRCOSY spectrum of PEO (M_w = 8000 g/mol) in capsule dispersion obtained after inverse Laplace transformation.

in capsule dispersion. Two sharp peaks are identified, with maxima at the same relaxation time T_2, but with clearly different diffusion coefficients. The T_2 relaxation time obtained from the DRCOSY experiment is 0.45 ± 0.10 s, which is identical to the value obtained from the conventional relaxation measurement of PEO in capsule dispersion (see Table 2). The larger error of the DRCOSY result is due to limited resolution of the inverse Laplace transformation. The diffusion coefficients of PEO (M_w = 8000 g/mol), extracted from the DRCOSY experiments are $D_A = (4.8 \pm 0.9) \times 10^{-11}$ m^2 s^{-1} and $D_B = (9.6 \pm 0.5) \times 10^{-13}$ m^2 s^{-1}. They agree to the apparent diffusion coefficients found in the PFG-NMR experiment, see Table 2. Similar results with a similar agreement are observed for PEO chains with the other molecular weights.

Though the quantitative results of DRCOSY experiments, i.e., the population fractions and the distribution of different diffusion coefficients and relaxation times, are of limited precision, it can be confirmed that PEO is distributed between two sites. In particular, the T_2 values in both sites do not differ. This proves the presence of encapsulated chains with relaxation times

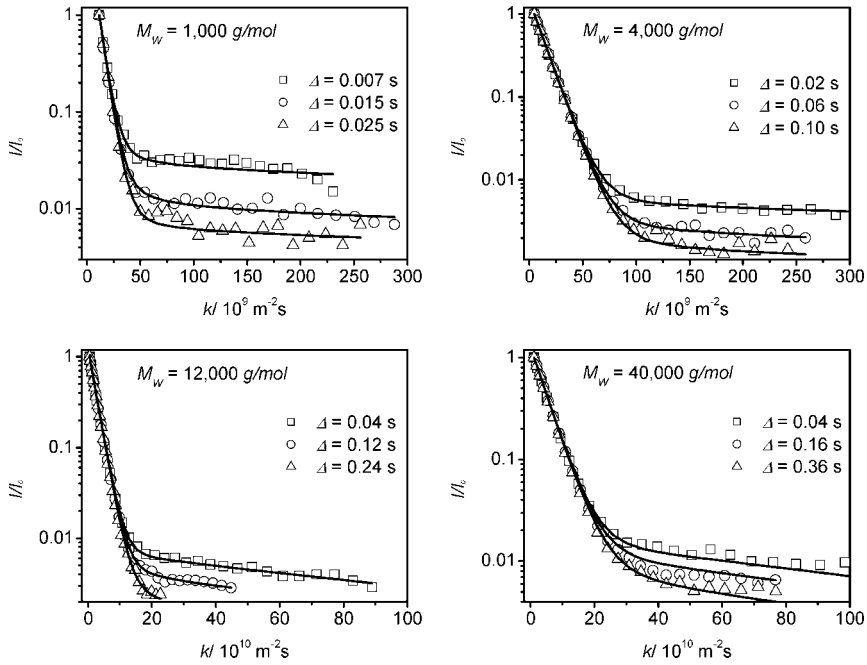

Figure 4. Echo decay curves of the PFG stimulated echo sequence for different observation times. The solid lines are the result of a global fit of all echo decays for the same molecular weight. Resulting parameters are given in the Table 3.

identical to those of free chains. It further implies that the chain mobility on segmental scale as well as on the local bond scale is the same in either site. The same mobility of free and encapsulated chains indicates that the encapsulated chains are situated within the capsule core without interactions with or absorption into the capsule wall.

In conclusion, the DRCOSY data have demonstrated that the Δ-dependence of the population fraction of the encapsulated site, Figure 2, can be clearly attributed to the effect of molecular exchange rather than a relaxation effect. To quantify the exchange dynamics, the Δ-dependent diffusion echo decays are analyzed in the two-site model.

Analysis of Diffusion and Exchange. The model of intermediate exchange between two sites, eqs 7 and 9, is employed. We point out that no assumptions about the time scales or regimes of exchange are made in the analysis. Fixed parameters are the diffusion coefficient and the relaxation times T_1 and T_2 of PEO in the free site, where the values of free chains in D_2O are taken from Table 1. The diffusion coefficient of encapsulated chains, D_B, is assumed to be that of the capsule itself, since any motion of a chain within the capsule interior leads to negligible mean square displacements as compared to the mean square displacement of the capsule itself. It is calculated from the Stokes−Einstein relation, eq 12. The radius of the capsule is assumed to be that of the silica particle before dissolution, $R = 200$ nm, as given by the manufacturer and confirmed by dynamic light scattering. Then, the calculated diffusion coefficient of the capsule is $D_B = (9.2 \pm 0.7) \times 10^{-13}$ m^2 s^{-1}, in agreement with the preliminary biexponential fits, Figure 2 and Table 2. T_1 and T_2 are assumed to be identical in both sites, which is well supported by the DRCOSY results. T_{2A} and T_{2B} are fixed parameters given by the CPMG and DRCOSY experiments, thus it is $T_{2A} = T_{2B} = (0.45 \pm 0.05)$ s. The set of fixed input parameters is thus $P_{in} = (D_A, D_B, T_{1A}, T_{2A}, T_{1B}, T_{2B})$. The diffusion data are analyzed in a global fit of all echo decays determined for one molecular weight and different Δ. A global set of floating parameters $P_{res} = (\tau_A, \tau_B)$ is optimized to fit the set of echo decay curves with the global set of fixed input parameters P_{in}.

TABLE 3: Bound Fractions f_B and Exchange Times τ_{ex} for Different Molecular Weights of PEO, Calculated from the Fit Results (τ_A, τ_B)

M_w(g/mol)	f_B	τ_{ex} (s)
1000	0.010 ± 0.002	0.005 ± 0.001
2000	0.010 ± 0.002	0.013 ± 0.003
4000	0.011 ± 0.002	0.034 ± 0.005
8000	0.010 ± 0.001	0.087 ± 0.005
12 000	0.010 ± 0.002	0.122 ± 0.008
20 000	0.012 ± 0.001	0.147 ± 0.010
40 000	0.014 ± 0.001	0.185 ± 0.008

In Figure 4 the global fits of the diffusion data are shown for a selection of different molecular weights of PEO. Similar results are obtained for the data sets of the remaining molecular weights (data not shown). The model describes the experimental data very well. From the resulting parameters τ_A and τ_B, the bound fraction, f_B, and the exchange time, τ_{ex}, of PEO are calculated, using eqs 5 and 6, respectively. The results are given in Table 3 together with their respective errors. These errors include the errors of all input parameters and are obtained from evaluating the fit results under variation of all input parameters in their respective error range.

Discussion

The fraction of encapsulated chains is close to 0.01, and it is independent of molecular weight. This fraction is on the order of the volume fraction occupied by capsules, which is ∼2% of the total volume. It has to be noted that the capsule concentration of ∼2% vol is calculated from the initial amount of particles employed for multilayer coating. Due to the possibility of losses of particles or capsules in the decant−redispersion processes, the true particle concentration is probably somewhat lower than 2%.

The exchange time τ_{ex} calculated from the fit results shows a strong dependence on molecular weight. Permeation rate constants k_{ex} can be calculated as $k_{ex} = 1/\tau_{ex}$ and are strongly decreasing with increasing chain length, see Figure 5.

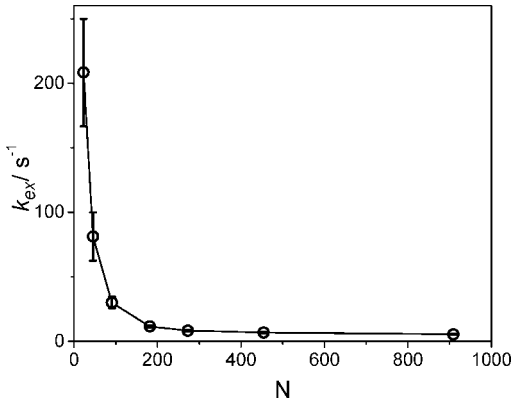

Figure 5. Rate constants $k_{ex} = 1/\tau_{ex}$ for molecular exchange through the capsule wall as calculated from the exchange times given in Table 3.

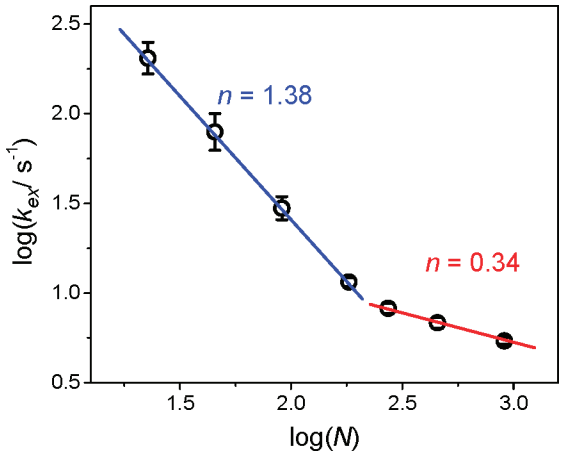

Figure 6. Log−log representation of the exchange rate in dependence on chain length. Straight lines are fits of a power law in the respective length range, with the resulting exponents displayed.

Short chains ($N < 200$, i.e. $M_w < 10\,000$ g/mol) show a strong dependence of the exchange rates on N. For longer chains, the dependence of the exchange rate on chain length is less pronounced. In order to analyze the molecular weight dependence in terms of a scaling law, the exchange rate is given in a log−log representation in Figure 6. Here, the existence of two regimes, which imply distinctly different mechanisms for the permeation process, is evident. In both regimes the dependence in the log−log representation of Figure 6 is linear, and thus either regime can be described by a power law for τ_{ex} according to eq 1 with a scaling exponent n. Values of n obtained from fits with this power law are 1.38 and 0.34 for the regimes below and above a molecular weight of 10 000 g/mol, respectively. Within error these exponents agree to $^4/_3$ and $^1/_3$.

The data suggest the dominance of two different mechanisms for short and for long chains, respectively. A potential explanation is depicted in Figure 7: In the short chain regime there could be a permeation process that does not require chain unfolding, while a long chain has to unfold in order to pass through a pore.

Possibly the pore size distribution in the wall plays a role, such that the penetration does not take place through monodisperse holes, which are small compared to R_H. If large pores are present, their size distribution has to be considered as well. Pore size distributions in polyelectrolyte multilayers were determined by cryoporometry, which resulted in pores of 1 to 1.5 nm size;[20]

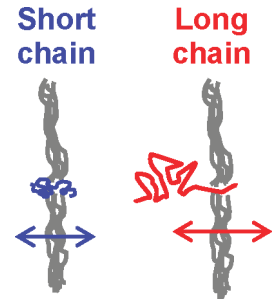

Figure 7. Sketch of potential permeation mechanisms of short chains and long chains, respectively.

furthermore, permeation experiments of small rigid solutes resulted in a size cutoff of about or little less than 1 nm.[18,19] These sizes are comparable to the hydrodynamic radius of the PEO (which is 1.1−3.5 nm (Table 1)). All these experiments yielding nanometer sizes were performed on multilayers that had not been subject to template dissolution, a process which was shown to modify the structure of the wall due to large osmotic pressure differences occurring in template dissolution.[42] Thus, in hollow capsule walls the original pore sizes in the nanometer range might well be accompanied by larger pores.

Nevertheless, though a polydispersity of pore sizes might play a role, the transition between two regimes is clearly pronounced. The crossover between two different scaling behaviors occurs at a molecular weight of 10 000 g/mol, i.e., a number of repeat units of $N = 227$. In the regime of long chains, the molecular weight dependence is less pronounced. Very likely, the long chains with $R_H >$ pore size have to unfold prior to their migration through the porous layer, see Figure 7.

In comparison to the theoretical predictions obtained from various kinds of simulations, see introduction, our experimental exponents are clearly much smaller than those suggested by literature.[3,6] However, differences between the experimental situation and the assumptions for the theoretical models have to be considered, thus making the comparison difficult: In the experiment any free chain has to undergo a series of processes in order to be transferred to the other side of the membrane: (i) Diffusive transport to the vicinity of the wall is necessary, (ii) a chain end or loop has to find a suitable pore and has to be inserted into it, and then (iii) the chain has to diffuse through the pore at the cost of chain entropy until finally, when the chain center has reached the pore, (iv) the remainder of the chain is transferred. In the simulations of translocation, the typical starting situation is a chain sticking halfway in the wall and the translocation time describes the process of the release to one side. This corresponds to process iv of the experimental situation only. While diffusive transport to the wall is typically fast, it can be expected that processes ii and iii have an influence on the overall scaling law. In lack of theoretical descriptions of these processes, a full comparison remains difficult.

Conclusions

Nuclear magnetic resonance with pulsed field gradients represents a powerful approach for the observation of molecular exchange through the porous wall of hollow capsules. Polyethylene oxide molecules of various molecular weights are used as probe for the observation of the exchange process through the polyelectrolyte capsule wall under equilibrium conditions. A quantitative analysis of the diffusion data with the model of intermediate exchange between two sites is done, where the number of free parameters is decreased due to the prior

information obtained from DRCOSY experiments. For small polyethylene oxide chains ($M_w < 10\,000$ g/mol), the analysis yields a very strong dependence of the exchange rate on the probe molecule chain length. With molecular masses increasing above $M_w = 10\,000$ g/mol, the slope of the plot decreases by almost 1 order of magnitude, indicating a second mechanism of permeation. In both regimes the permeation time obeys a scaling law in dependence on chain length with exponents of $^4/_3$ and $^1/_3$ for short and long chains, respectively. These exponents represent the full process of permeation through the membrane, and are much smaller than exponents derived from theoretical descriptions of the final step of translocation of a chain through the pore.

Acknowledgment. We thank the group of G. Schmitz (Material Physics), in particular D. Baither, for TEM measurements to control the capsule quality. R.P.C. is thankful to the "International Graduate School of Chemistry at the University of Münster" for a doctoral fellowship.

References and Notes

(1) Muthukumar, M. *J. Chem. Phys.* **1999**, *111*, 10371.
(2) Park, P. J.; Sung, W. *J. Chem. Phys.* **1998**, *108*, 3013.
(3) Dubbeldam, J. L. A.; Milchev, A.; Rostiashvili, V. G.; Vilgis, T. A. *Phys. Rev. E* **2007**, *76*, 010801.
(4) Dubbeldam, J. L. A.; Milchev, A.; Rostiashvili, V. G.; Vilgis, T. A. *EPL* **2007**, *79*, 18002.
(5) Chuang, J.; Kantor, Y.; Kardar, M. *Phys. Rev. E* **2002**, *65*, 011802.
(6) Luo, K.; Ala-Nissila, T.; Ying, S. C. *J. Chem. Phys.* **2006**, *124*, 034714.
(7) Romiszowski, P.; Sikorski, A. *Comput. Mater. Sci.* **2007**, *38*, 533.
(8) Huopaniemi, I.; Luo, K.; Ala-Nissila, T. *J. Chem. Phys.* **2006**, *125*, 124901.
(9) Panja, D.; Barkema, G. T.; Ball, R. C. *J. Phys.-Cond. Mat.* **2007**, *19*, 432202.
(10) Keyser, U. F.; Koeleman, B. N.; Van Dorp, S.; Krapf, D.; Smeets, R. M. M.; Lemay, S. G.; Dekker, N. H.; Dekker, C. *Nat. Phys.* **2006**, *2*, 473.
(11) Storm, A. J.; Storm, C.; Chen, J. H.; Zandbergen, H.; Joanny, J. F.; Dekker, C. *Nano Lett.* **2005**, *5*, 1193.
(12) Donath, E.; Sukhorukov, G. B.; Caruso, F.; Davis, S. A.; Möhwald, H. *Angew. Chem., Int. Ed.* **1998**, *37*, 2202.
(13) Sukhorukov, G. B.; Donath, E.; Moya, S.; Susha, A. S.; Voigt, A.; Hartmann, J.; Möhwald, H. *J. Microencaps.* **2000**, *17*, 177.
(14) Antipov, A. A.; Sukhorukov, G. B.; Donath, E.; Möhwald, H. *J. Phys. Chem. B* **2001**, *105*, 2281.
(15) Dai, J. H.; Jensen, A. W.; Mohanty, D. K.; Erndt, J.; Bruening, M. L. *Langmuir* **2001**, *17*, 931.
(16) Ostrander, J. W.; Mamedov, A. A.; Kotov, N. A. *J. Am. Chem. Soc.* **2001**, *123*, 1101.
(17) Petrov, A. I.; Antipov, A. A.; Sukhorukov, G. B. *Macromolecules* **2003**, *36*, 10079.
(18) Liu, X. Y.; Bruening, M. L. *Chem. Mater.* **2004**, *16*, 351.
(19) Jin, W. Q.; Toutianoush, A.; Tieke, B. *Appl. Surf. Sci.* **2005**, *246*, 444.
(20) Vaca Chávez, F.; Schönhoff, M. *J. Chem. Phys.* **2007**, *126*, 104705.
(21) Sukhorukov, G. B.; Brumen, M.; Donath, E.; Möhwald, H. *J. Phys. Chem. B* **1999**, *103*, 6434.
(22) Antipov, A. A.; Sukhorukov, G. B.; Möhwald, H. *Langmuir* **2003**, *19*, 2444.
(23) Glinel, K.; Sukhorukov, G. B.; Möhwald, H.; Khrenov, V.; Tauer, K. *Macromol. Chem. Phys.* **2003**, *204*, 1784.
(24) Schönhoff, M.; Söderman, O. *J. Phys. Chem. B* **1997**, *101*, 8237.
(25) Wohlgemuth, M.; Mayer, C. *J. Colloid Interface Sci.* **2003**, *260*, 324.
(26) Boissier, C.; Löfroth, J. E.; Nyden, M. *J. Phys. Chem. B* **2003**, *107*, 7064.
(27) Bauer, A.; Hauschild, S.; Stolzenburg, M.; Forster, S.; Mayer, C. *Chem. Phys. Lett.* **2006**, *419*, 430.
(28) Waldeck, A. R.; Lennon, A. J.; Chapman, B. E.; Kuchel, P. W. *J. Chem. Soc., Faraday Trans.* **1993**, *89*, 2807.
(29) Waldeck, A. R.; Kuchel, P. W.; Lennon, A. J.; Chapman, B. E. *Prog. NMR Spectr.* **1997**, *30*, 39.
(30) Moniot, K. I.; Kuchel, P. W. *Concepts Magn. Reson. Part A* **2003**, *19A*, 51.
(31) Adalsteinsson, T.; Dong, W. F.; Schönhoff, M. *J. Phys. Chem. B* **2004**, *108*, 20056.
(32) Qiao, Y.; Galvosas, P.; Adalsteinsson, T.; Schönhoff, M.; Callaghan, P. T. *J. Chem. Phys.* **2005**, *122*, 214912.
(33) Choudhury, R. P.; Schönhoff, M. *J. Chem. Phys.* **2007**, *127*, 234702.
(34) Schwarz, B.; Schönhoff, M. *Colloid Surf. A* **2002**, *198*, 293.
(35) Godefroy, S.; Callaghan, P. T. *Magn. Reson. Imaging* **2003**, *21*, 381.
(36) Callaghan, P. T.; Godefroy, S.; Ryland, B. N. *J. Magn. Reson.* **2003**, *162*, 320.
(37) Stilbs, P. *Progr. NMR Spectrosc.* **1987**, *19*, 1.
(38) Kärger, J. *Adv. Colloid Interface Sci.* **1985**, *23*, 129.
(39) Price, W. S. *Annu. Rep. NMR Spectrosc.* **1996**, *32*, 51.
(40) Kärger, J. *Ann. Phys.* **1971**, *27*, 107.
(41) Doi, M.; Edwards, S. F. *The theory of polymer dynamics*; Oxford University Press: Oxford, U.K., 1986.
(42) Dong, W. F.; Ferri, J. K.; Adalsteinsson, T.; Schönhoff, M.; Sukhorukov, G. B.; Möhwald, H. *Chem. Mater.* **2005**, *17*, 2603.

JP804680Q